Acta Crystallographica Section C
Crystal Structure Communications
ISSN 0108-2701

1-(β-D-Erythrofuranosyl)adenosine

Paul C. Kline,[a] Hongqiu Zhao,[b] Bruce C. Noll,[b] Allen G. Oliver[b] and Anthony S. Serianni[b]*

[a]Department of Chemistry, Middle Tennessee State University, Murfreesboro, TN 37132, USA, and [b]Department of Chemistry and Biochemistry, University of Notre Dame, Notre Dame, IN 46556, USA
Correspondence e-mail: aseriann@nd.edu

Received 21 December 2009
Accepted 2 March 2010
Online 19 March 2010

The title compound, also known as β-erythroadenosine, $C_9H_{11}N_5O_3$, (I), a derivative of β-adenosine, (II), that lacks the C5′ exocyclic hydroxymethyl (–CH_2OH) substituent, crystallizes from hot ethanol with two independent molecules having different conformations, denoted (I*A*) and (I*B*). In (I*A*), the furanose conformation is ${}^{O}T_1$–E_1 (C1′-*exo*, east), with pseudorotational parameters *P* and τ_m of 114.4 and 42°, respectively. In contrast, the *P* and τ_m values are 170.1 and 46°, respectively, in (I*B*), consistent with a ${}^{2}E$–${}^{2}T_3$ (C2′-*endo*, south) conformation. The *N*-glycoside conformation is *syn* (+*sc*) in (I*A*) and *anti* (−*ac*) in (I*B*). The crystal structure, determined to a resolution of 2.0 Å, of a cocrystal of (I) bound to the enzyme 5′-fluorodeoxyadenosine synthase from *Streptomyces cattleya* shows the furanose ring in a near-ideal ${}^{O}E$ (east) conformation (*P* = 90° and τ_m = 42°) and the base in an *anti* (−*ac*) conformation.

Comment

In a recent report, the crystal structure of the ribonucleoside derivative 1-(β-D-erythrofuranosyl)cytidine (β-erythrocytidine), (III), was determined and its structural parameters compared with those of β-cytidine, β-erythrouridine and β-uridine (Kline *et al.*, 2007). This prior work is extended in the present investigation to the title compound, (I), which lacks the exocyclic C5′ hydroxymethyl group found in β-adenosine, (II).

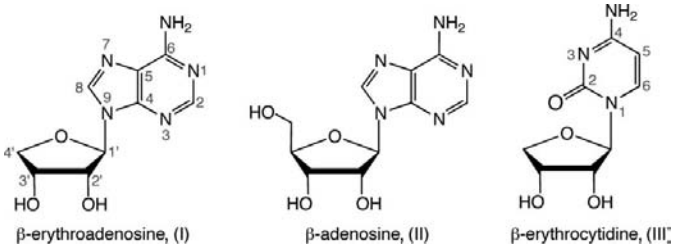

Solution NMR studies of (I) and (II) have revealed significant differences in the furanose conformation. The ${}^{3}J_{H1,H2}$, ${}^{3}J_{H2,H3}$ and ${}^{3}J_{H3,H4S}$ spin-couplings in (I) are 6.7, 4.6 and 1.7 Hz, respectively, whereas the corresponding values in (II) are 6.2, 5.3 and 3.3 Hz, respectively (Kline & Serianni, 1992). Pseudorotational analysis of these NMR couplings shows that (I) greatly prefers a south conformation (∼95%) (for definitions, see Fig. 1), with *P* = 180.1° and τ_m = 40°. For (II), a greater proportion of the north form was found (∼23%; *P* = 19.1° and τ_m = 38°), and the predominant south form (∼77%) had *P* = 153.3° and τ_m = 38°.

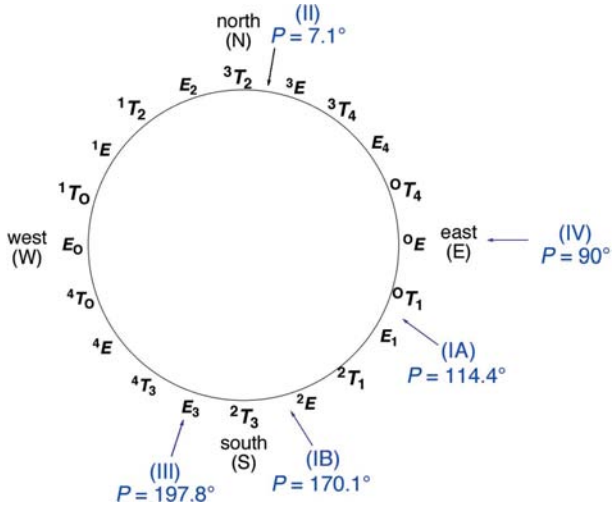

Figure 1
Pseudorotational itinerary of furanose rings in nucleosides, showing the *P* values for compounds (I)–(IV).

The crystal structure of (I) (Fig. 2) contains two molecules with different conformations in the asymmetric unit, denoted (I*A*) and (I*B*). In (I*A*), the furanose conformation is ${}^{O}T_1$–E_1 (C1′-*exo*, east), with pseudorotational parameters *P* = 114.4° and τ_m = 42° (Table 1). This conformation is best described as an east form in the pseudorotational itinerary (Fig. 1). For (I*B*), *P* = 170.1° and τ_m = 46°, consistent with a ${}^{2}E$–${}^{2}T_3$ (C2′-*endo*, south) conformation (Fig. 1). The latter geometry, which is observed in the common biologically relevant nucleosides/nucleotides, is structurally similar to that observed in the crystal structure of β-erythrocytidine, (III) (*P* = 197.8° and τ_m = 44°) (Fig. 1). In comparison, β-adenosine, (II), crystallizes in a ${}^{3}T_2$–${}^{3}E$ (C3′-*endo*, north; *P* = 7.1° and τ_m = 37°) confor-

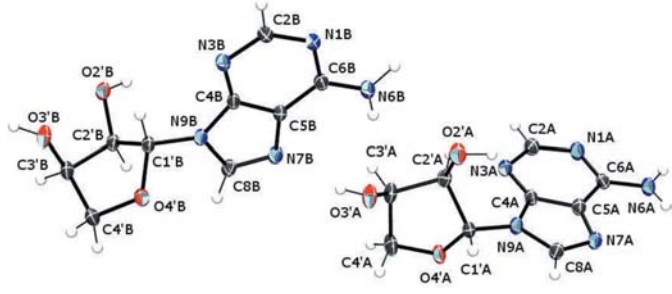

Figure 2
The molecular structures of (I*A*) (atom labels with suffix A) and (I*B*) (atom labels with suffix B), showing the atom-numbering scheme. Displacement ellipsoids are drawn at the 50% probability level and H atoms are shown as small spheres of arbitrary radii.

 doi:10.1107/S0108270110008024

mation (Fig. 1). The degree of ring puckering in erythronucleosides (I) and (III), embodied in the τ_m parameter (44±2°), is significantly greater than that observed in (II) (37°), suggesting that removal of the bulky –CH_2OH substituent allows greater furanose ring deformation from planarity. This trend also emerged from prior NMR *J*-coupling analysis (Kline & Serianni, 1992), although the difference is smaller.

The furanose ring conformation influences the conformation about the *N*-glycoside linkage. The adenine base assumes an *anti* (−*ac*) conformation [O4′—C1′—N9—C4 = −114.5 (3)°] in (I*B*), having the furanose ring in a south (^2E) conformation (Table 1). Shifting the furanose conformation towards the east forms, as observed in (I*A*), causes a radical change in the *N*-glycoside conformation to the *syn* (+*sc*) conformation [O4′—C1′—N9—C4 = 68.4 (3)°]; the quasi-equatorial C1′—N9 bond in the E_1 furanose structure readily accommodates this conformation. It should be noted that a similar *N*-glycoside conformation is observed in (III) (*syn*, +*sc*), where the furanose conformation is E_3, suggesting that *syn* conformations can be accommodated in a wider range of furanose conformations in erythronucleosides than in ribo- and 2′-deoxyribonucleosides, in which base interactions with the bulky –CH_2OH substituent at C4′ limit access to the more sterically demanding *syn* state. In (II), a north (^3E) furanose conformation correlates with an *anti* (*ap*) *N*-glycoside conformation [O4′—C1′—N9—C4 = −171.4°], as expected (Table 1). While the preferred *N*-glycoside conformation in (I) in solution is currently unknown, these results, and those previously reported (Kline *et al.*, 2007), suggest that an equilibrium mixture of both *syn* and *anti* geometries might be expected.

Prior studies (Westhof & Sundaralingam, 1983) have demonstrated the interdependencies between *P*, τ_m and endocyclic torsion angles in furanose rings. We tested these correlations using data from (I*A*), (I*B*) and (III), given that their constituent furanose ring conformations have *P* values in the range 114–198° with very similar τ_m values. The experimentally observed trends in the C4′—O4′—C1′, O4′—C1′—C2′, C2′—C3′—C4′ and C3′—C4′—O4′ bond angles are well predicted using the Westhof–Sundaralingam correlations. For example, the C2′—C3′—C4′ and C3′—C4′—O4′ bond angles are smallest in (III) and largest in (I*A*) (Table 1), consistent with the predicted trend. Likewise, the small value of the C4′—O4′—C1′ bond angle in (I*A*) relative to those found in (I*B*) and (III) (Table 1) fulfills predictions based on the observed differences in ring conformation.

A similar treatment of bond lengths in (I)–(III) is complicated by differences in both furanose and *N*-glycoside conformations. Moderate differences of 0.018–0.024 Å are observed for bonds C1′—C2′, C1′—O4′ and C4′—O4′, and larger differences of ∼0.032 Å are found for bonds C2′—C3′ and C3′—C4′ (Table 1). The last two bonds are significantly extended in (I*A*), presumably due to its unique furanose conformation and/or to the *syn* geometry of its *N*-glycosidic linkage.

The crystal structure, determined to a resolution of 2.0 Å, of a cocrystal of (I) with the enzyme 5′-fluorodeoxyadenosine synthase, (IV), from *Streptomyces cattleya* (Cobb *et al.*, 2006), shows that the enzyme binds to (I) in a furanose conformation (^OE, east; P = 90° and τ_m = 42°) similar to that observed in (I*A*), but in an *N*-glycoside conformation (*anti*, −*ac*) similar to that observed in (I*B*) (Table 1).

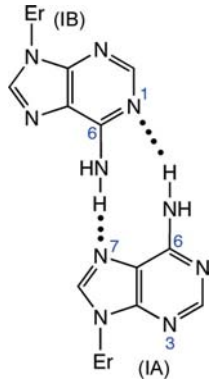

Figure 3
Non-Watson–Crick hydrogen bonding (dotted lines) observed between the bases of (I*A*) and (I*B*) (Er is the β-D-erythrofuranosyl ring).

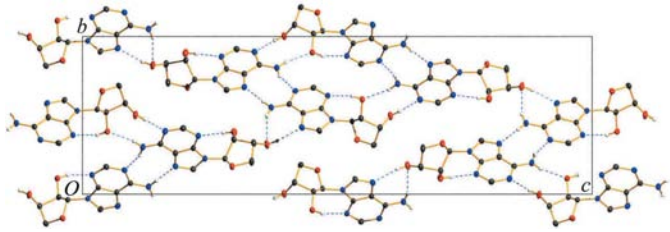

Figure 4
Hydrogen-bonding scheme (dashed lines) of (I), viewed down the *a* axis.

The furanose rings of (I*A*) and (I*B*) display different intermolecular hydrogen-bonding motifs (see Table 2). In (I*A*), atom O2′*A* serves as a donor to atom N3*A* of an adjacent (I*A*) unit. Atom O3′*A* of (I*A*) serves as a donor to atom N7*B* of (I*B*), while atom O3′*A* serves as an acceptor to amine atom N6*B* of (I*B*); in both cases, the (I*B*) molecule is that found in the same asymmetric unit. Atom O4′*A* is not involved in hydrogen bonding, and atom O2′*A* does not serve as an acceptor in (I*A*). In (I*B*), atom O2′*B* serves as a donor to atom N3*B* of an adjacent (I*B*) unit, and atom O2′*B* serves as an acceptor to amine atom N6*A* of an adjacent (I*A*) unit. Atom O3′*B* serves as a donor to atom N1*A* of the same adjacent (I*A*) unit. Atom O4′*B* is not involved in hydrogen bonding, and atom O3′*B* does not serve as an acceptor in (I*B*). No intramolecular hydrogen bonds are found in (I*A*) or (I*B*).

Intermolecular base–base (non-Watson–Crick) hydrogen bonding is also present in (I). Amine atom N6*A* (donor) and atom N7*A* (acceptor) of (I*A*) are hydrogen bonded to atom N1*B* (acceptor) and amine atom N6*B* (donor), respectively, of an adjacent (I*B*) molecule (Fig. 3 and Table 2). No base–base hydrogen bonding is observed in the crystal structures of (II) and (III).

The crystal packing of (I) consists of units of the base–base hydrogen-bonded pairs of (I*A*) and (I*B*) described above. These base–base hydrogen-bonded pairs extend the structure

through contacts from the hydroxy group to nearby adenosine N atoms of other nearby base–base pairs. The adenosine amine N atoms (N6*A* and N6*B*) not only form the base–base pair unit, but also form hydrogen bonds to nearby hydroxy groups (Fig. 4). The overall packing is a three-dimensional hydrogen-bonded network of pairs of (I*A*) and (I*B*) molecules. The layers of adenosine moieties adopt a herringbone arrangement within the lattice.

Experimental

Compound (I) was prepared as described previously (Kline & Serianni, 1992) and crystallized from hot ethanol.

Crystal data

$C_9H_{11}N_5O_3$
M_r = 237.23
Orthorhombic, $P2_12_12_1$
a = 4.793 (3) Å
b = 11.365 (7) Å
c = 36.79 (2) Å
V = 2004 (2) Å^3
Z = 8
Synchrotron radiation
λ = 0.77490 Å
μ = 0.12 mm^{-1}
T = 150 K
0.12 × 0.04 × 0.02 mm

Data collection

Bruker APEXII CCD area-detector diffractometer
Absorption correction: multi-scan (*SADABS*; Sheldrick, 2008*a*)
T_{min} = 0.986, T_{max} = 0.998
23772 measured reflections
2910 independent reflections
2556 reflections with $I > 2\sigma(I)$
R_{int} = 0.112

Refinement

$R[F^2 > 2\sigma(F^2)]$ = 0.047
$wR(F^2)$ = 0.126
S = 1.07
2910 reflections
307 parameters
H-atom parameters constrained
$\Delta\rho_{max}$ = 0.34 e Å^{-3}
$\Delta\rho_{min}$ = −0.31 e Å^{-3}
Absolute structure: Flack (1983), with 2059 Friedel pairs
Flack parameter: 1.2 (11)

There are two crystallographically independent molecules in the asymmetric unit, differing in their rotation about the furanose–adenine bond. H atoms were located in difference Fourier maps and subsequently geometrically idealized and refined as riding, with C—H = 0.95–1.00 Å, N—H = 0.88 Å and O—H = 0.84 Å, and with U_{iso}(H) = 1.2U_{eq}(C,N,O).

Although the absolute structure parameter [1.2 (11); Flack, 1983] is indicative of the inverted absolute configuration, this is an unreliable measure at the wavelength of radiation used (0.7749 Å), especially for a light-atom structure [a detailed discussion of this problem can be found in Hooft *et al.* (2008)]. The correct configuration was therefore assigned from the known chirality of the molecule in question.

Data collection: *APEX2* (Bruker, 2007); cell refinement: *SAINT* (Bruker, 2007); data reduction: *SAINT*; program(s) used to solve structure: *SHELXS97* (Sheldrick, 2008*b*); program(s) used to refine structure: *SHELXL97* (Sheldrick, 2008*b*); molecular graphics: *XP* in *SHELXTL* (Sheldrick, 2008*b*) and *POV-RAY* (Cason, 2003); software used to prepare material for publication: *enCIFer* (Allen *et al.*, 2004) and *publCIF* (Westrip, 2010).

Samples for synchrotron crystallographic analysis were submitted through the SCrALS (Service Crystallography at Advanced Light Source) program. Crystallographic data were

Table 1
Comparison of structural parameters in (I*A*), (I*B*), (II) and (III).

	(IA)	(IB)	(II)†	(III)	(IV)†
Bond lengths (Å)					
C1′—C2′	1.540 (4)	1.531 (4)	1.530	1.548 (3)	1.544
C2′—C3′	1.561 (4)	1.542 (3)	1.528	1.528 (3)	1.547
C3′—C4′	1.542 (4)	1.530 (4)	1.522	1.512 (3)	1.546
C1′—N1′				1.475 (2)	
C1′—N9′	1.455 (3)	1.459 (3)	1.467		1.465
C1′—O4′	1.420 (3)	1.435 (3)	1.411	1.414 (3)	1.445
C4′—O4′	1.456 (3)	1.469 (3)	1.450	1.452 (3)	1.445
C2′—O2′	1.413 (3)	1.413 (3)	1.411	1.414 (3)	1.429
C3′—O3′	1.428 (3)	1.425 (3)	1.418	1.422 (2)	1.430
C2—O2				1.234 (3)	
C4—N4				1.335 (3)	
C6—N6	1.330 (3)	1.338 (3)	1.332		1.384
Bond angles (°)					
C4′—O4′—C1′	105.3 (2)	108.2 (2)	110.48	108.24 (14)	105.3
O4′—C1′—N1				110.6	
O4′—C1′—N9	108.2 (2)	108.15 (19)	109.31		110.3
O4′—C1′—C2′	105.1 (2)	104.9 (2)	107.29	107.04 (16)	104.9
C1′—C2′—C3′	102.0 (2)	99.3 (2)	101.36	100.67 (15)	104.0
C2′—C3′—C4′	103.6 (2)	99.95 (19)	102.72	99.78 (15)	104.0
C3′—C4′—O4′	107.3 (2)	105.8 (2)	104.66	104.69 (18)	104.8
C1′—N1—C2				121.52 (18)	
C1′—N1—C6				117.92 (17)	
C1′—N9—C4	129.5 (2)	126.4 (2)	124.26		126.2
C1′—N9—C8	124.6 (2)	127.4 (2)	130.01		126.3
Torsion angles (°)					
O4′—C1′—N1—C2				60.8 (2) (*syn*, +*sc*)	
O4′—C1′—N1—C6				−120.29 (18)	
O4′—C1′—N9—C4	68.4 (3) (*syn*, +*sc*)	−114.5 (3) (*anti*, −*ac*)	−171.38 (*anti*, *ap*)		−158.0 (*anti*, −*ac*)
O4′—C1′—N9—C8	−112.9 (3)	58.0 (3)	9.92		22.0
C2′—C1′—N1—C2				−60.6 (3)	
C2′—C1′—N1—C6				118.28 (19)	
C2′—C1′—N9—C4	−48.5 (4)	128.2 (3)	70.11		86.5
C2′—C1′—N9—C8	130.2 (3)	−59.3 (3)	−108.59		−93.4
C1′—C2′—C3′—C4′	−17.0 (3)	−44.5 (2)	35.76	−40.83 (18)	0.0
C2′—C3′—C4′—O4′	−6.7 (3)	33.0 (3)	−32.48	42.1	−24.0
C3′—C4′—O4′—C1′	30.3 (3)	−7.3 (3)	15.92	−26.19 (19)	40.5
C4′—O4′—C1′—C2′	−41.9 (3)	−22.1 (3)	7.44	−0.97 (18)	−40.4
O4′—C1′—C2′—C3′	36.3 (3)	42.0 (2)	−27.30	27.00 (18)	23.8
N1—C2—N3—C4				−4.6 (3)	
N1—C6—C5—C4				−2.9 (3)	
N9—C4—N3—C2	178.8 (3)	−179.9 (3)	178.44		180.0
N9—C8—N7—C5	−0.6 (3)	0.3 (3)	0.41		−0.3
Furanose					
P (°)	114.4 E_1, C1′-*exo*	169.8 ^2E, C2′-*endo*	7.1 ^3E, C3′-*endo*	197.8 E_3, C3′-*exo*	89.7 ^OE, O1′-*endo*
τ_m (°)	42	46	37	44	42

† Standard uncertainties unavailable.

Table 2
Hydrogen-bond geometry (Å, °).

D—H···A	D—H	H···A	D···A	D—H···A
N6A—H6A···O2′B^{i}	0.88	2.14	2.988 (3)	162
N6A—H6B···N1B^{ii}	0.88	2.11	2.957 (4)	161
O2′A—H2′C···N3A^{iii}	0.84	2.17	2.999 (3)	171
O2′B—H2′D···N3B^{iv}	0.84	2.00	2.807 (3)	162
O3′A—H3′C···N7B	0.84	2.02	2.820 (3)	158
N6B—H6C···N7A^{v}	0.88	2.05	2.934 (3)	177
N6B—H6D···O3′A	0.88	2.20	3.011 (4)	152
O3′B—H3′D···N1A^{vi}	0.84	1.96	2.798 (3)	175

Symmetry codes: (i) $-x+\frac{3}{2}, -y+2, z+\frac{1}{2}$; (ii) $-x, y-\frac{1}{2}, -z+\frac{1}{2}$; (iii) $x-1, y, z$; (iv) $x+1, y, z$; (v) $-x, y+\frac{1}{2}, -z+\frac{1}{2}$; (vi) $-x+\frac{3}{2}, -y+2, z-\frac{1}{2}$.

collected on Beamline 11.3.1 at the Advanced Light Source (ALS), Lawrence Berkeley National Laboratory. The ALS is supported by the US Department of Energy, Office of Energy Sciences, under contract No. DE-AC02-05CH11231.

Supplementary data for this paper are available from the IUCr electronic archives (Reference: GT3016). Services for accessing these data are described at the back of the journal.

References

Allen, F. H., Johnson, O., Shields, G. P., Smith, B. R. & Towler, M. (2004). *J. Appl. Cryst.* **37**, 335–338.

Bruker (2007). *APEX2* (Version 2.1-4) and *SAINT* (Version 7.34A). Bruker Nonius AXS Inc., Madison, Wisconsin, USA.

Cason, C. J. (2003). *POV-RAY*. Persistence of Vision Raytracer Pty. Ltd, Victoria, Australia.

Cobb, S. L., Deng, H., McEwan, A. R., Naismith, J. H., O'Hagan, D. & Robinson, D. A. (2006). *Org. Biomol. Chem.* **4**, 1458–1460.

Flack, H. D. (1983). *Acta Cryst.* A**39**, 876–881.

Hooft, R. W. W., Straver, L. H. & Spek, A. L. (2008). *J. Appl. Cryst.* **41**, 96–103.

Kline, P. C., Noll, B. C., Zhao, H. & Serianni, A. S. (2007). *Acta Cryst.* C**63**, o137–o140.

Kline, P. C. & Serianni, A. S. (1992). *J. Org. Chem.* **57**, 1772–1777.

Sheldrick, G. M. (2008*a*). *SADABS*. Version 2007/4. University of Göttingen, Germany.

Sheldrick, G. M. (2008*b*). *Acta Cryst.* A**64**, 112–122.

Westhof, E. & Sundaralingam, M. (1983). *J. Am. Chem. Soc.* **105**, 970–976.

Westrip, S. P. (2010). *publCIF*. In preparation.